Supplementary Information for

Irreversibility of winter precipitation over the Northeastern Pacific and Western North America against CO_2 forcing

Zhenhao Xu[1,2,3], Yu Kosaka[2*], Masaki Toda[2,4], Tomoki Iwakiri[5,6], Gang Huang[1,3*], Fei Ji[7,8], Ayumu Miyamoto[2,9], and Weichen Tao[1]

1. State Key Laboratory of Numerical Modeling for Atmospheric Sciences and Geophysical Fluid Dynamics, Institute of Atmospheric Physics, Chinese Academy of Sciences, Beijing, China.
2. Research Center for Advanced Science and Technology, The University of Tokyo, Tokyo, Japan.
3. University of Chinese Academy of Sciences, Beijing, China.
4. Max-Planck Institute for Meteorology, Hamburg, Germany.
5. Atmosphere and Ocean Research Institute, The University of Tokyo, Chiba, Japan.
6. Meteorological Research Institute, Ibaraki, Japan.
7. College of Atmospheric Sciences, Lanzhou University, Lanzhou, China.
8. Collaborative Innovation Center for Western Ecological Safety, Lanzhou University, Lanzhou, China.
9. Scripps Institution of Oceanography, University of California, San Diego, La Jolla, CA, USA.

**** Corresponding authors:***

Dr. Yu Kosaka,

E-mail : ykosaka@atmos.rcast.u-tokyo.ac.jp

Research Center for Advanced Science and Technology, The University of Tokyo

Dr. Gang Huang,

E-mail : hg@mail.iap.ac.cn

Institute of Atmospheric Physics, Chinese Academy of Sciences

Submitted to ***npj climate and atmospheric science***

October 28th, 2024

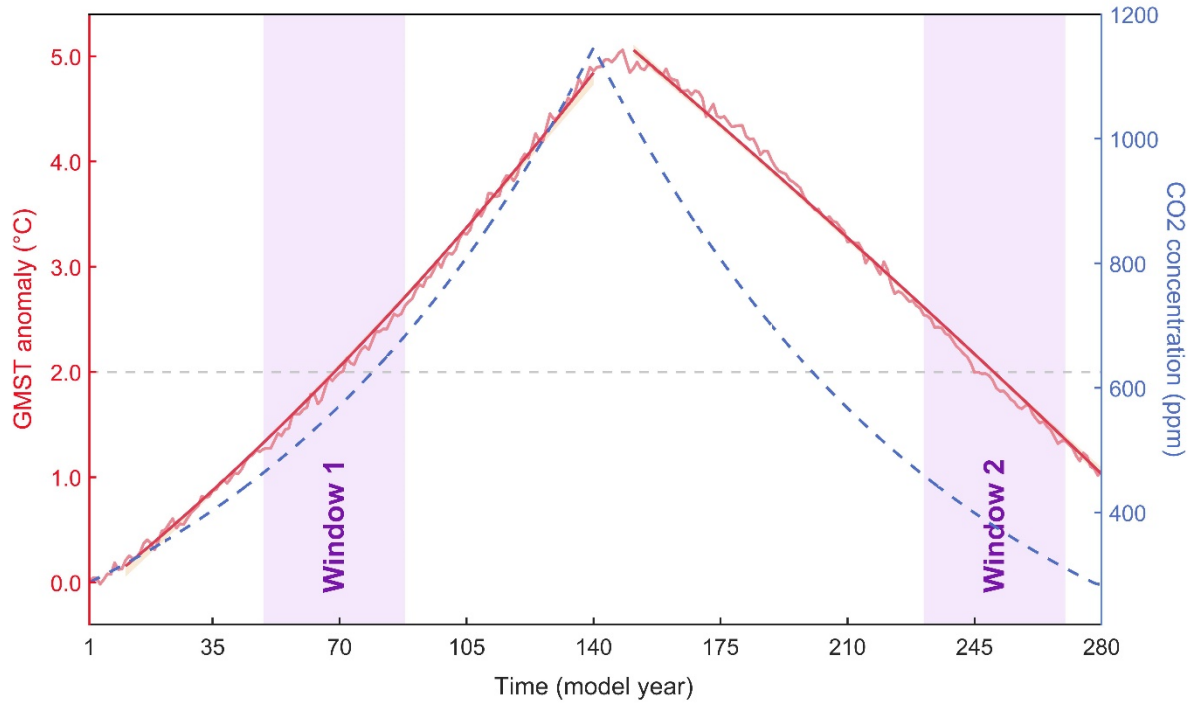

Supplementary Fig. 1 | Same as Figure 1 (a), but from CMIP6 multi-model ensemble mean, with 40-year-long windows located.

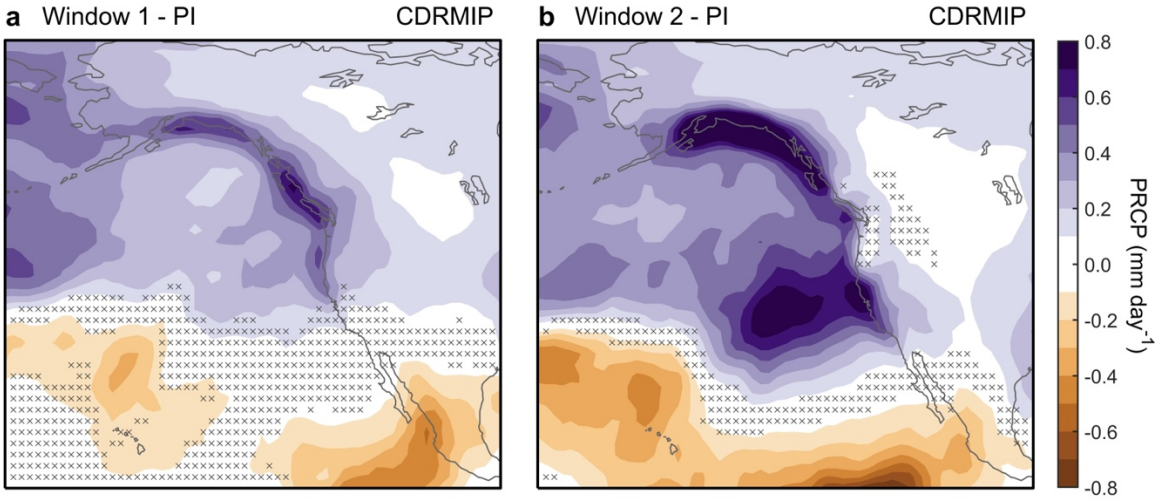

Supplementary Fig. 2 | Same as Figure 2 (f) and (g), but based on the CMIP6 CDRMIP multi-model ensemble mean. Crosses denote insignificant using the two-sided Student's *t*-test at a 95% confidence level.

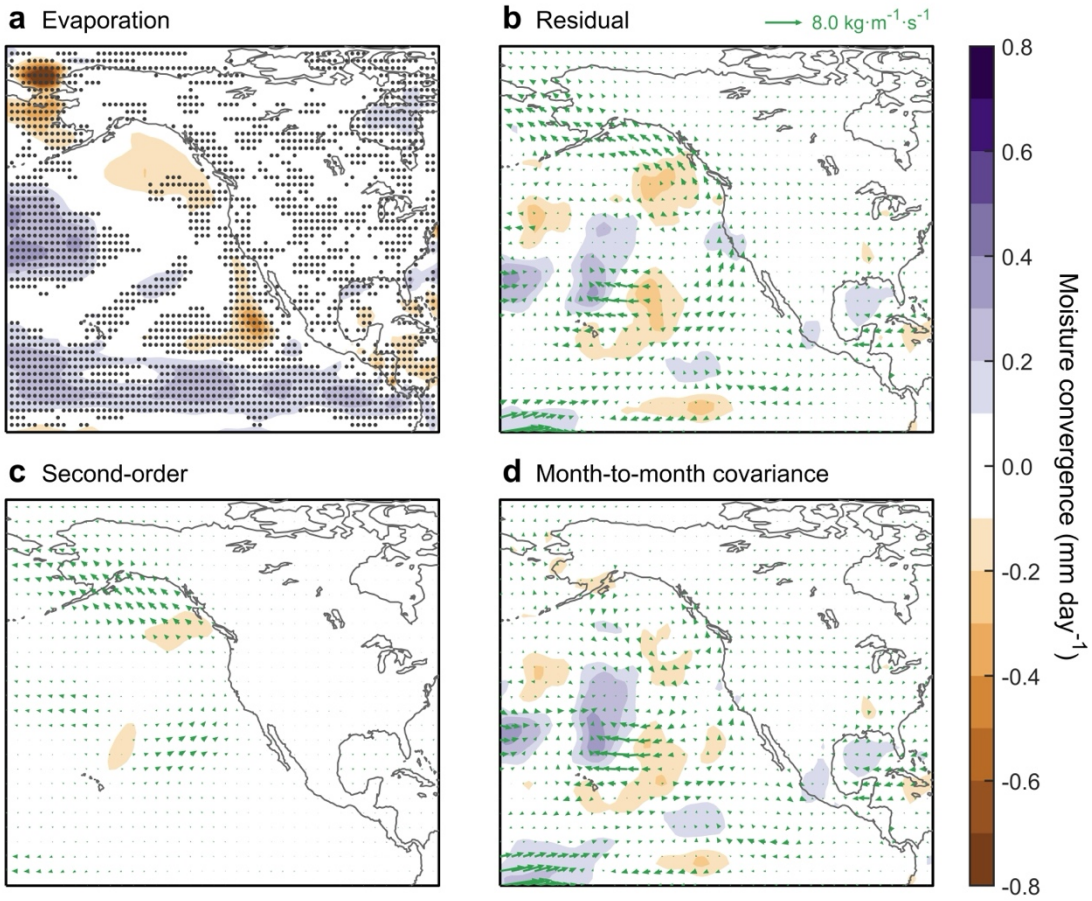

Supplementary Fig. 3 | Asymmetric response of the evaporation (**a**), residual term (**b**; identical to Fig. 3f), second-order term (**c**), and month-to-month covariance term (**d**) from the atmospheric moisture budget analysis applied to MIROC6 (see Methods for details). Black dots in **a** indicate at least four of five members (80%) agree with the sign of the ensemble mean. Vectors in **b-d** show moisture flux.

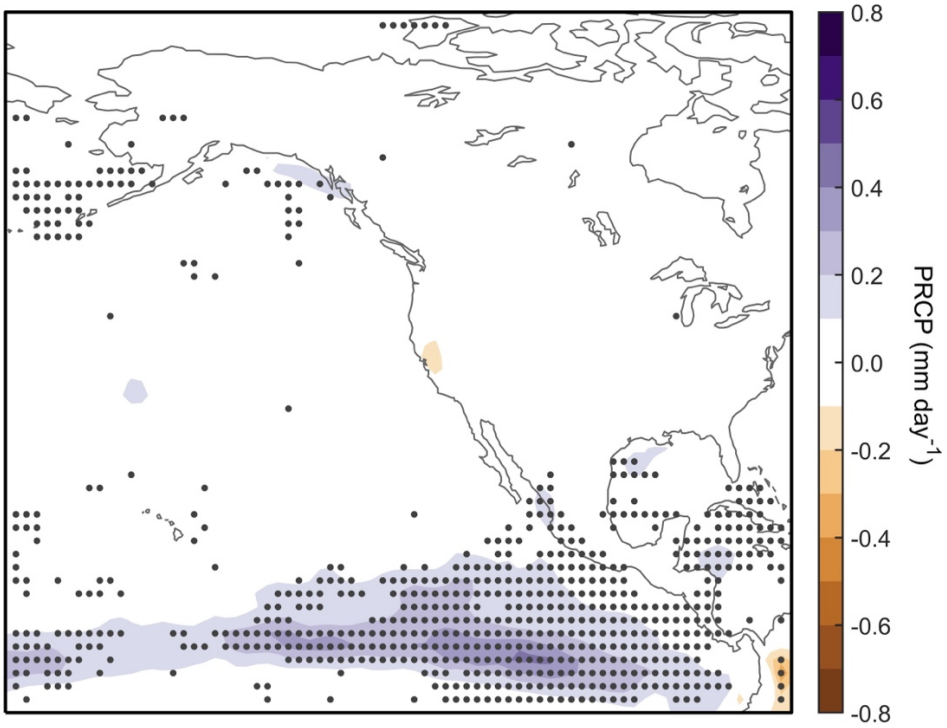

Supplementary Fig. 4 | Asymmetric change in winter precipitation over the NPWNA region induced by the CO_2 direct effect estimated with the MIROC6 Hansen experiment. Black dots indicate that at least two-thirds of members agree with the sign of the ensemble mean.

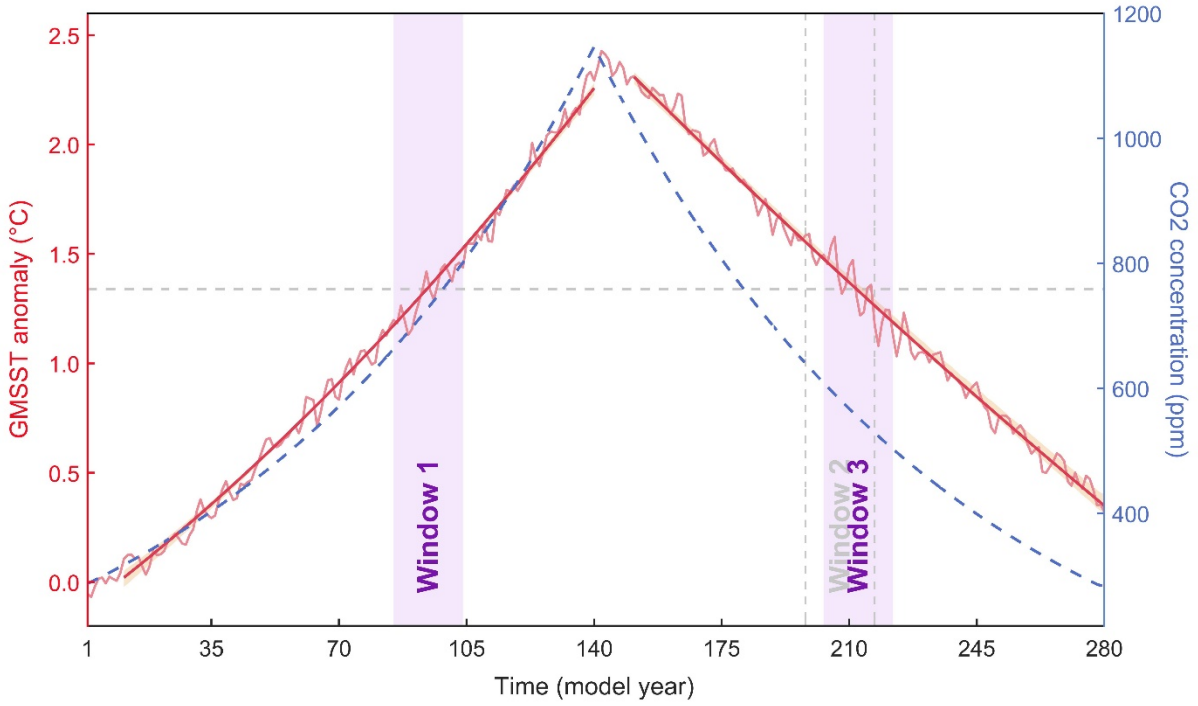

Supplementary Fig. 5 | Same as Fig. 1 (a), but for GMSST. Note that Window 3 (Year 203-222; right purple shading) has the same GMSST increase as Window 1 (Year 85-104; left purple shading). The gray vertical lines indicate Window 2 (Year 198-217).

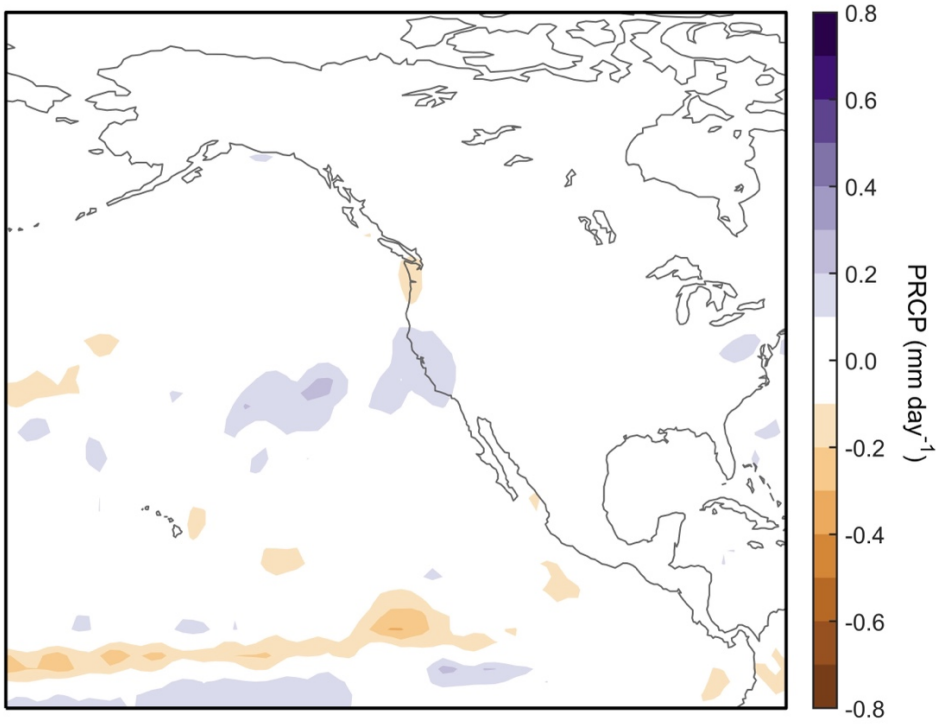

Supplementary Fig. 6 | Asymmetric change in winter precipitation over the NPWNA region induced by the GMSST difference in MIROC6. Note that no change in the NPWNA region passes the two-sided Student's *t*-test at a 90% confidence level.

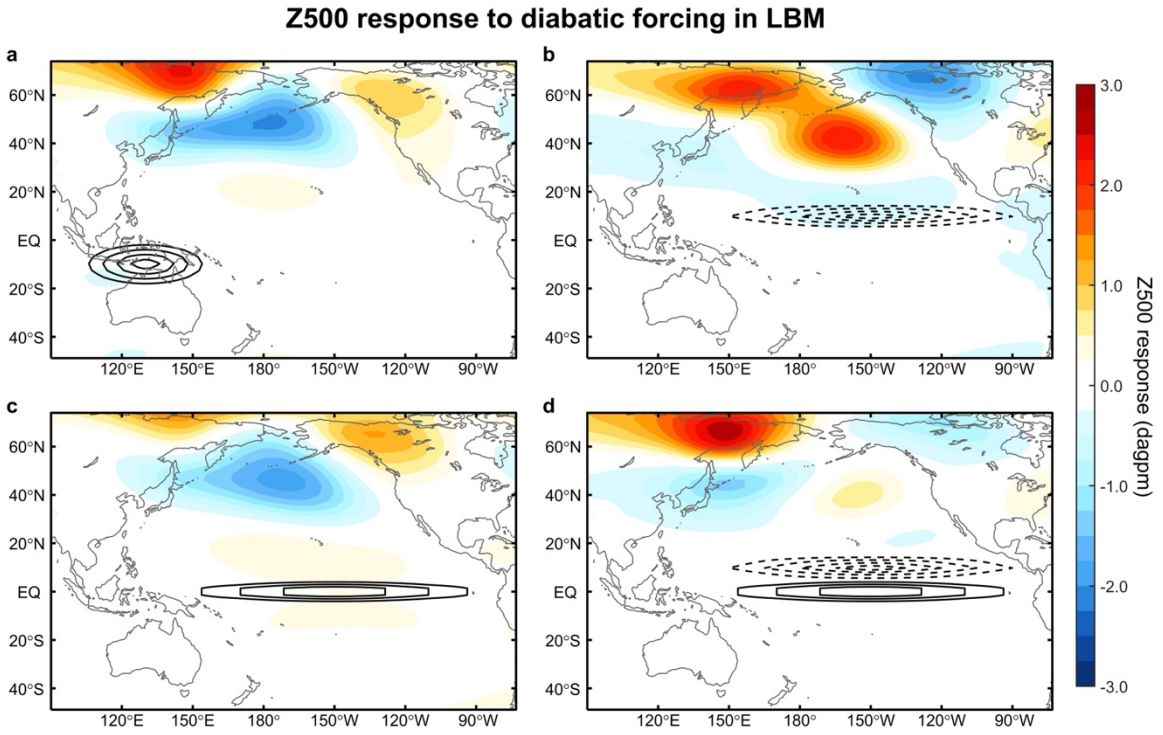

Supplementary Fig. 7 | Steady response to imposed diabatic forcing in the LBM. Shadings represent the response of the 500 hPa geopotential height (unit: dagpm) to the diabatic heating in the north of Australia (**a**), cooling in the north off-equatorial central-eastern Pacific (**b**), and heating in the equatorial central-eastern Pacific (**c**). The subplot **d** shows the sum of **b** and **c**. Solid (dashed) contours indicate the prescribed diabatic heating (cooling) at $\sigma = 0.45$ with intervals of 0.2 K day^{-1} (zero line is omitted for clarity).

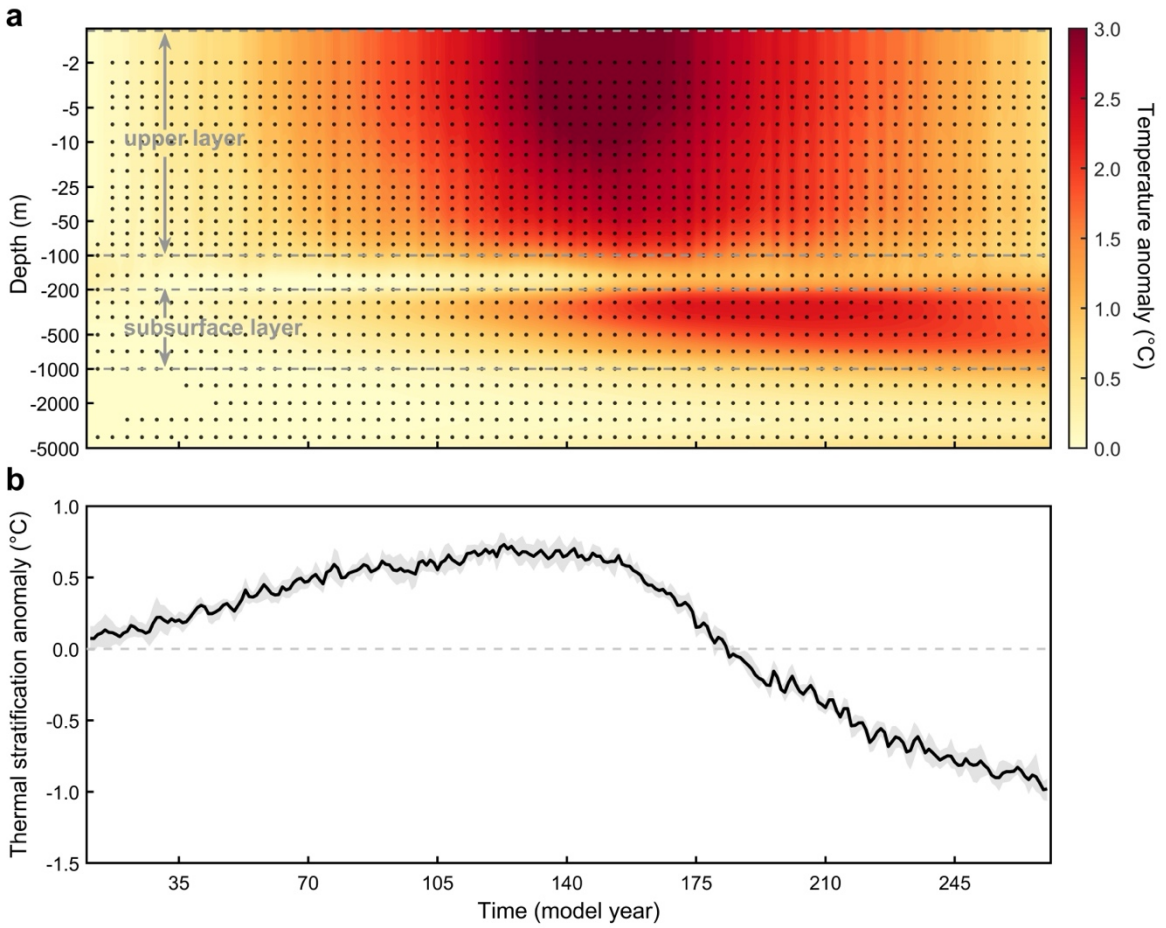

Supplementary Fig. 8 | Nonlinear evolution of ocean thermal stratification in the tropical eastern Pacific during boreal winter in a symmetric changing CO_2 pathway in MIROC6. **a,** Temporal evolution of the vertical profile of ocean potential temperature over the tropical central-eastern Pacific (5°S-5°N, 180°-80°W). Note non-uniform vertical grid interval. Black dots indicate that at least four of five members (80%) agree with the sign of the ensemble mean. **b,** Time series of the stratification index defined as the difference of potential temperature anomalies between the upper layer (above 100 m) and sub-surface layer (200-1000 m). The gray shading indicates the 95% confidence interval based on the bootstrap method.

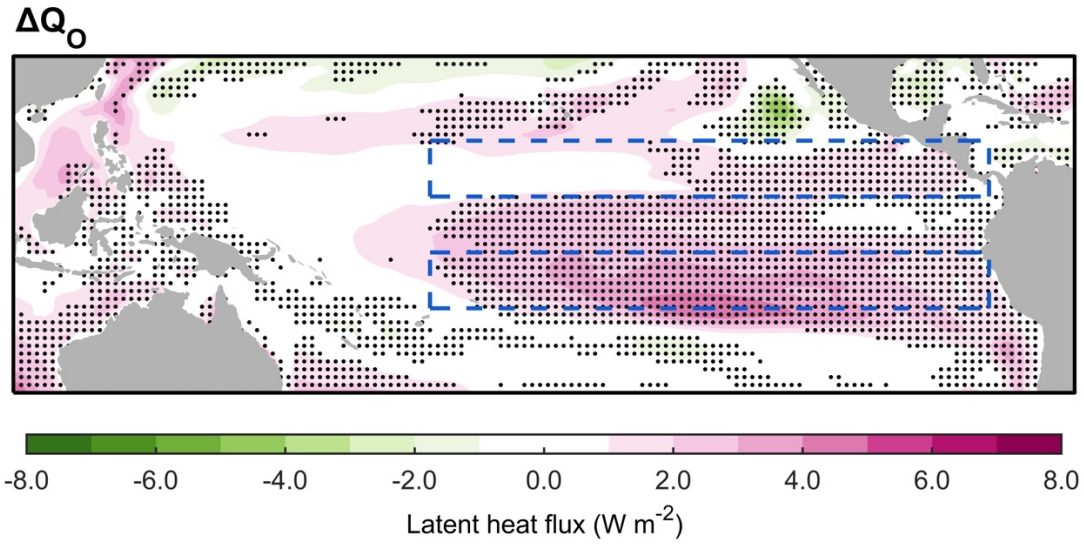

Supplementary Fig. 9 | Asymmetric response of the latent heat flux in MIROC6 during boreal winter due to the SST dependence of evaporation (see Methods for details). Black dots indicate at least four of five members (80%) agree with the sign of the ensemble mean. Blue boxes are the same as those in Fig. 5.

Supplementary Table 1. Lists of the eight CMIP6 CDRMIP models used in this study with experiment details.

Model Name	Country (Center)	Var label	Model year			Reference
			piControl	1pctCO_2	1pctCO_2-cdr	
ACCESS-ESM1-5	Australian (CSIRO)	r1i1p1f1	0101-1000	101-250	241-1000	(Ziehn et al. 2020)
CanESM5	Canada (CCCma)	r1i1p2f1	5550-6600	1850-2000	1991-2290	(Swart et al. 2019)
CESM2	America (NCAR)	r1i1p1f1	001-999	001-150	001-2000	(Danabasoglu et al. 2020)
CNRM-ESM2-1	France (CNRM-CERFACS)	r1i1p1f2	1850-2349	1850-1999	1990-2189	(Séférian et al. 2019)
GFDL-ESM4	America (GFDL)	r1i1p1f1	001-500	001-150	141-340	(Dunne et al. 2019)
MIROC-ES2L	Japan (JAMSTEC/NIES/AORI)	r1i1p1f2	1850-2349	1850-1999	1989-2490	(Hajima et al. 2020)
NorESM1-LM	Norway (NCC)	r1i1p1f1	1600-2100	001-150	141-399	(Seland et al. 2020)
UKESM1-0-LL	UK (MOHC)	r1i1p1f2	1960-3839	1850-1999	1990-2639	(Sellar et al. 2019)

Supplementary References

1. Danabasoglu, G. et al. The Community Earth System Model Version 2 (CESM2). *J. Adv. Model. Earth Syst.* **12**, e2019MS001916 (2020).
2. Dunne, J. P. et al. The GFDL Earth System Model Version 4.1 (GFDL-ESM 4.1): Overall coupled model description and simulation characteristics. *J. Adv. Model. Earth Syst.* **12**, e2019MS002015 (2020).
3. Hajima, T. et al. Development of the MIROC-ES2L Earth system model and the evaluation of biogeochemical processes and feedbacks. *Geosci. Model Dev.* **13**, 2197–2244 (2020).
4. Séférian, R. et al. Evaluation of CNRM Earth-System model, CNRM-ESM2-1: role of Earth system processes in present-day and future climate. *J. Adv. Model. Earth Syst.* **11**, 4182–4227 (2019).
5. Seland, Ø. et al. Overview of the Norwegian Earth System Model (NorESM2) and key climate response of CMIP6 DECK, historical, and scenario simulations. *Geosci. Model Dev.* **13**, 6165–6200 (2020).
6. Sellar, A. A. et al. Implementation of U.K. Earth system models for CMIP6. *J. Adv. Model. Earth Syst.* **12**, e2019MS001946 (2020).
7. Swart, N. C. et al. The Canadian Earth System Model version 5 (CanESM5.0.3). *Geosci. Model Dev.* **12**, 4823–4873 (2019).
8. Ziehn, T. et al. The Australian Earth System Model: ACCESS-ESM1.5, *J. South. Hemisphere Earth Syst. Sci.* **70**, 193-214 (2020).